

# Fibroglandular tissue distribution in the breast during mammography and tomosynthesis based on breast CT data: A patient-based characterization of the breast parenchyma

Christian Fedon\* and Marco Caballo\*

*Department of Medical Imaging, Radboud University Medical Center, 6500 HB Geert Grooteplein-Zuid, Nijmegen, The Netherlands*

Eloy García

*Vall d' Hebron Institute of Oncology (VHIO), Barcelona, Spain*

Oliver Diaz

*Department of Mathematics and Computer Science, University of Barcelona, Barcelona, Spain*

*CIMD, Parc Taulí Hospital Universitari, Institut d'Investigació i Innovació Parc Taulí, Sabadell, Spain*

John M. Boone

*Department of Radiology and Biomedical Engineering, University of California Davis Health, 4860 "Y" Street, suite 3100 Ellison building, Sacramento, CA 95817, USA*

David R. Dance

*National Co-ordinating Centre for the Physics of Mammography, NCCPM, Royal Surrey County Hospital, Guildford GU2 7XH, UK*

*Department of Physics, University of Surrey, Guildford GU2 7XH, UK*

Ioannis Sechopoulos<sup>a)</sup>

*Department of Medical Imaging, Radboud University Medical Center, 6500 HB Geert Grooteplein-Zuid, Nijmegen, The Netherlands*

*Dutch Expert Centre for Screening (LRCB), PO Box 6873, Nijmegen 6503 GJ, The Netherlands*

(Received 17 June 2020; revised 30 October 2020; accepted for publication 7 January 2021; published 3 February 2021)

**Purpose:** To develop a patient-based breast density model by characterizing the fibroglandular tissue distribution in patient breasts during compression for mammography and digital breast tomosynthesis (DBT) imaging.

**Methods:** In this prospective study, 88 breast images were acquired using a dedicated breast computed tomography (CT) system. The breasts in the images were classified into their three main tissue components and mechanically compressed to mimic the positioning for mammographic acquisition of the craniocaudal (CC) and mediolateral oblique (MLO) views. The resulting fibroglandular tissue distribution during these compressions was characterized by dividing the compressed breast volume into small regions, for which the median and the 25th and 75th percentile values of local fibroglandular density were obtained in the axial, coronal, and sagittal directions. The best fitting function, based on the likelihood method, for the median distribution was obtained in each direction.

**Results:** The fibroglandular tissue tends to concentrate toward the caudal (about 15% below the mid-line of the breast) and anterior regions of the breast, in both the CC- and MLO-view compressions. A symmetrical distribution was found in the MLO direction in the case of the CC-view compression, while a shift of about 12% toward the lateral direction was found in the MLO-view case.

**Conclusions:** The location of the fibroglandular tissue in the breast under compression during mammography and DBT image acquisition is a major factor for determining the actual glandular dose imparted during these examinations. A more realistic model of the parenchyma in the compressed breast, based on patient image data, was developed. This improved model more accurately reflects the fibroglandular tissue spatial distribution that can be found in patient breasts, and therefore might aid in future studies involving radiation dose and/or cancer development risk estimation. © 2021 The Authors. *Medical Physics* published by Wiley Periodicals LLC on behalf of American Association of Physicists in Medicine. [<https://doi.org/10.1002/mp.14716>]

Key words: breast cancer risk, breast imaging, compressed breast, dosimetry, fibroglandular tissue

## 1. INTRODUCTION

The amount and distribution of fibroglandular tissue is a relevant topic in the breast cancer imaging realm. A high amount of fibroglandular tissue in the breast is recognized as an independent risk factor for breast cancer.<sup>1,2</sup> In addition, mammograms of dense breasts, that is, breasts that are composed of a

high percentage of fibroglandular tissue, result in lower sensitivity and specificity for detection of suspicious lesions, due to the higher risk of tissue masking.<sup>3</sup>

The distribution of the fibroglandular tissue, that is, its actual three-dimensional (3D) location within the breast, is one of the main factors that determines the actual patient breast dose.<sup>4-6</sup> During acquisition of a mammogram or

digital breast tomosynthesis (DBT) image, fibroglandular tissue that is located close to the upper surface of the compressed breast may receive a dose an order of magnitude higher than tissue located at the lowest portion of the breast. However, we currently ignore this factor during dosimetry and risk estimations, using only a model that assumes that the fibroglandular tissue is uniformly distributed throughout the entire breast.<sup>7</sup> Developing a patient-based model of this distribution would allow to obtain more accurate estimates of the average glandular dose during imaging, known to currently overestimate the patient dose by an average of 30%.<sup>4-6</sup> In addition, gaining knowledge on the “average” fibroglandular distribution could provide additional insight for improved risk models, beyond simply considering the overall amount of dense tissue in the breast, as done by current models of risk of breast cancer development.<sup>8,9</sup>

Characterizing the amount and distribution of fibroglandular tissue in patient breasts, especially during compression, has been a challenging task.<sup>10-12</sup> Such characterization is inherently limited by the two-dimensional (2D) nature of mammography, and the poor vertical resolution of DBT.<sup>13</sup> Only recently, the development of dedicated breast CT<sup>14</sup> has allowed for the true 3D depiction and characterization of breast anatomy with high, isotropic spatial resolution.<sup>15</sup> Analysis of a large number of patient breast CT images has provided insight into the fibroglandular tissue distribution in the uncompressed breast.<sup>5</sup> Importantly, this information was enough to validate breast density estimation algorithms, opening the door to new insights on the amount of fibroglandular tissue present in compressed breasts.<sup>16</sup> However, the actual distribution of the fibroglandular tissue in the breast during compression for mammography and DBT imaging has still not been characterized.

Therefore, the aim of this study is to develop a patient-based model of the fibroglandular tissue distribution in compressed breasts using patient dedicated breast CT images. For this purpose, a simulation of mechanical compression using a biomechanical finite element model was used that mimicked the compression procedure during mammography and tomosynthesis.

## 2. MATERIALS AND METHODS

The fibroglandular tissue distribution in compressed breasts was analyzed as summarized in Fig. 1.

Briefly, after the acquisition of isotropic 3D images using a dedicated breast CT system, the voxels in the images were automatically classified, and the resulting breast representations underwent simulated mechanical compression via computer software. Finally, the internal tissue distribution in the classified, compressed breasts was analyzed in all three orthogonal directions.

### 2.A. Patient dataset

The patient image dataset used in this study was acquired with a dedicated breast CT system installed at Radboud university medical center (The Netherlands) as part of an unrelated clinical trial approved by the local medical ethics committee (approval number NL55378.091.15). The dataset, consisting of 115 images, was acquired between October 2016 and June 2019. All participants signed written informed consent, including the release of the research data, after anonymization, for other studies.

Women, 50 yr of age or older with a suspicious finding detected at mammographic screening (BI-RADS<sup>®</sup> 4 or 5) or

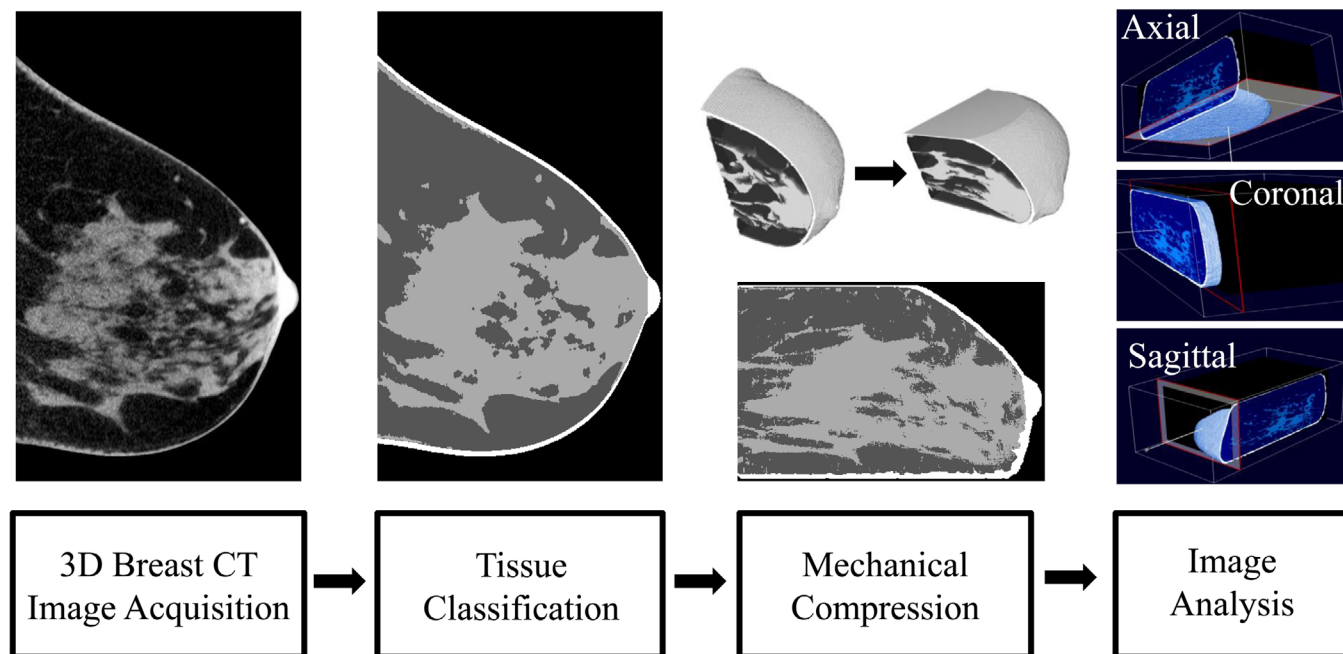


FIG. 1. Flowchart of the image processing pipeline to characterize the fibroglandular tissue distribution in the compressed breast. [Color figure can be viewed at [wileyonlinelibrary.com](http://wileyonlinelibrary.com)]

with a need for additional imaging (BI-RADS<sup>®</sup> 0), were eligible for the study (in the screening system in the Netherlands, BI-RADS<sup>®</sup> 4 or 5 can be assigned at screening). Exclusion criteria were suspected or confirmed pregnancy, bilateral mastectomy, the presence of the suspicious lesion in the axillary tail, prior breast cancer or breast biopsy in the recalled breast in the last 12 months, the presence of palpable lesions, breastfeeding, frailty, or inability to cooperate.

Biographic data and images were collected from each patient electronic medical record. In addition to the acquisition of the breast CT scans only as part of the research, patients also underwent two-view DBT examination of the same breast. The DBT examination was performed during the same visit as the breast CT acquisition, as part of the normal diagnostic work-up of the mammographic screening findings. Out of the 115 patient image dataset collected for that prospective trial, for this study, we extracted the cases where the subjects allowed the re-use of their data for additional research purposes, the images had no motion or other disturbing artifacts, and the entire breast fit in the field of view of a single breast CT image.

## 2.B. Image acquisition

The 3D breast images were acquired with the dedicated breast CT clinical prototype (Koning Corp., West Henrietta, NY, USA) installed at Radboud University Medical Center. The system has a source-to-imager distance of 92.3 cm and a source-to-isocenter distance of 65 cm. It is equipped with an x-ray tube with a W/AI anode/filter combination, which operates in a pulse mode (8 ms pulse) at a fixed tube voltage of 49 kV. The first half value layer is 1.39 mm Al, and the nominal focal spot 0.3 mm. The tube current for each patient breast is automatically selected by prior acquisition of two scout images normal to each other. A complete CT scan involves the acquisition of 300 projections over a full 360° revolution of the x-ray tube and detector (4030CB, Varian Medical System, Palo Alto, CA, USA) in 10 s, both of which simultaneously rotate under the prone patient. The CT scans were performed by trained breast imaging technologists and reconstructed using filtered backprojection (Shepp-Logan reconstruction filter) with isotropic cubic voxels of 0.273 mm.

## 2.C. Image segmentation and simulation of mechanical compression

Image tissue classification was performed on the 3D breast CT images following a previously described method developed by Caballo et al.,<sup>17</sup> after excluding the image slices containing the pectoral muscle. The method was used to classify each voxel in the reconstructed breast CT images into four categories (air, skin, adipose, and fibroglandular tissue), taking advantage of both intensity and regional information within the image.

Classified breast CT images were converted into a finite element biomechanical model in order to simulate the breast

compression performed during a mammographic and/or DBT procedure, following another process previously described by Fedon et al.<sup>18</sup> The mechanical compression was simulated with a previously described tool developed by García et al.<sup>19</sup> by moving the compression paddle toward the breast support until the desired breast thickness was reached. This value was equivalent to the compressed breast thickness recorded in the image header of the CC- or MLO-view DBT image of the corresponding breast. To mimic the CC acquisition, the compression was performed in the craniocaudal direction, while in the case of MLO acquisition the breast was compressed at a 45° angle to the CC compression. Breast laterality was taken into account by flipping the breast in order to have the correct orientation during the compression. All subsequent analyses, described in the next subsection, were performed after aligning the reference system (i.e., the coronal, axial, and sagittal views) with the direction of breast compression (0° for CC, 45° for MLO) (Fig. 2).

## 2.D. Fibroglandular tissue distribution characterization

To analyze the distribution of the fibroglandular tissue in the breast along the three anatomical planes (see Fig. 3), each resulting compressed breast volume was divided into 70 regions in each of the three orthogonal directions (i.e., axial, coronal, and sagittal). The number of regions was determined as a tradeoff between the optimal voxel size for dose evaluation, estimated to be below 2.5 mm per side, according to previous work,<sup>18</sup> and the increase in noise as the number of regions increases (resulting in each region being smaller).

For each of these views, the glandular fraction of the  $i$ -th region ( $GF_i$ ) was calculated as:

$$GF_i = \left( \frac{V_g}{V_g + V_a} \right)_i \quad (1)$$

where  $GF_i$  represent the glandularity for the  $i$ -th region, and  $V_g$  and  $V_a$  represent the number of fibroglandular and adipose voxels, respectively, in the  $i$ -th region.

The process was repeated for each classified-compressed image in our dataset, and the median, and the 25th and 75th percentiles of the GF in each region were calculated. The best-fitting function, based on the likelihood method, for the median distribution in each orthogonal direction was determined using the statistical software TableCurve 2D (Systat Software Inc., Chicago, IL, USA), and used to describe the fibroglandular distribution in our population.

## 2.E. Validation

Several additional investigations were performed to assess the appropriateness of our approach. First, a sensitivity analysis on the number of regions used to divide each breast into discrete locations was performed. To do so, the analysis as described above was repeated after setting the number of regions equal to 10, 30, 50, 100, and 130, and variations in

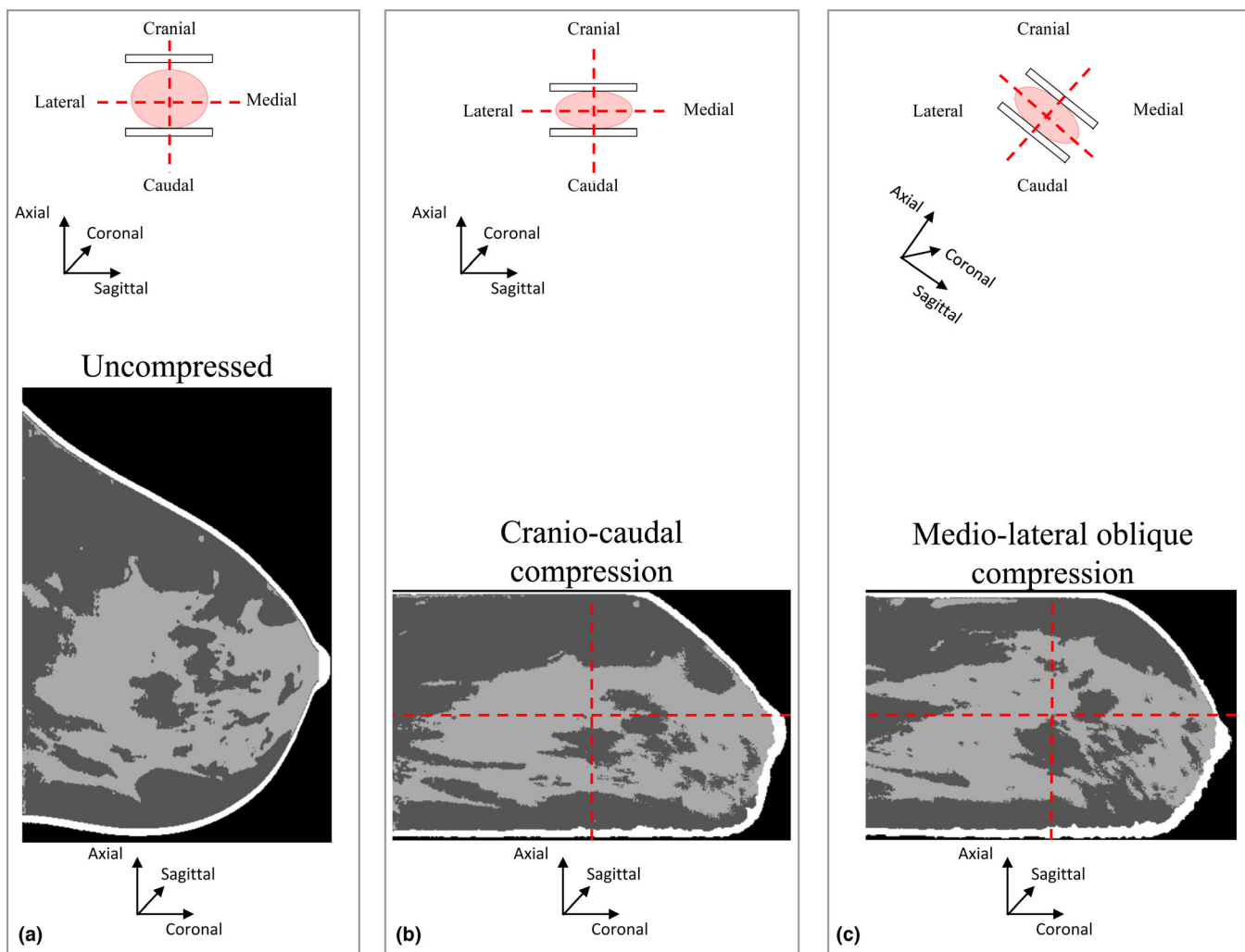


FIG. 2. Schematics of the frames of reference for all analyses performed in this study, (a) for the uncompressed breast CT data, and for (b) the CC and (c) MLO compressions. In each panel, the top part schematizes the breast positioning during mammography; the bottom part shows an example of classified breast CT image, before or after compression, with the respective frame of reference. [Color figure can be viewed at [wileyonlinelibrary.com](http://wileyonlinelibrary.com)]

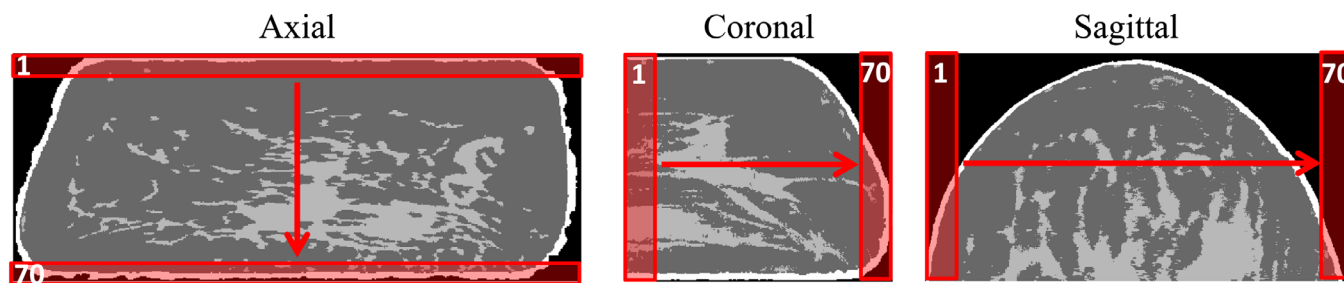


FIG. 3. Schematic of the regions used for the analysis of the fibroglandular tissue distribution along each of the orthogonal directions. The local fraction of fibroglandular tissue contained within each of the 70 regions in each of the three directions was determined after the breast underwent simulated mechanical compression. [Color figure can be viewed at [wileyonlinelibrary.com](http://wileyonlinelibrary.com)]

the extracted distributions were observed and compared to those obtained with 70 regions.

Second, to investigate any potential bias introduced by specific characteristics of the image dataset (and therefore to assess the appropriateness of the sample size), the analysis was repeated by stratifying the cases according to the

compressed breast thickness (<49 mm, 50 mm–69 mm, >70 mm), according to the presence or absence of mass-like lesions (to investigate their potential effect on the resulting fibroglandular tissue distribution), and according to the BI-RADS® breast density category (as assessed by the interpreting radiologist from the DM images, at diagnostic work-up).

These latter two analyses were performed for the CC view only. To detect any possible bias introduced by the compression procedure, the analysis was also performed on the uncompressed-classified breast model. This latter analysis was also compared with a previous study of Huang *et al.*,<sup>15</sup> where the fibroglandular distribution of 219 breast CT images was extracted along the coronal and the vertical section of the sagittal slice. These distributions were obtained with a different breast CT system and on a different patient population.

Finally, to investigate the accuracy in the simulation of the breast tissue displacement by the compression algorithm, the fibroglandular tissue distribution obtained from the compressed breast CT data was compared to that obtained by following the same process using the Volpara<sup>®</sup> (v1.5.4.0, Volpara Health Technologies Limited, Wellington, New Zealand) density maps derived from the respective patient mammograms. This software provides, given a raw input mammogram, a dense tissue map where each pixel indicates the height (in mm) of the fibroglandular tissue present between the compression paddle and the detector.<sup>20,21</sup>

To convert these representations to maps of glandular fraction by mass, a normalization by the compressed breast thickness was performed (after excluding a total of 3 mm of breast skin<sup>22</sup>), and the map pixel values were then converted into areal density fractions (which, for these purposes, are equivalent to mass fractions). Subsequently, to obtain the fibroglandular tissue distributions, the 70-region analysis described in the previous Section was performed in the two in-plane directions (coronal and sagittal). The analysis was performed only in the Volpara<sup>®</sup>-reported inner breast region, which is

estimated to be in contact with the compression paddle, and can be assumed to have a constant thickness density map.<sup>23</sup> That is, the breast edge region, where the thickness varies, and the area in the MLO-view images occupied by the pectoralis muscle, were excluded, since these regions do not allow for a reliable glandular fraction estimation. The analysis was performed for both the CC and MLO view, and the deriving distributions were compared to those obtained from the breast CT data. Furthermore, to quantify the similarity of the sagittal distributions, the experimental data were fitted with a Gaussian function, and the position of the peak, and the full-width-at-half-maximum, were identified and compared.

### 3. RESULTS

Out of the 115 cases in the existing dataset, 3 subjects had not allowed the re-use of their data for additional research purposes, 9 were excluded due to the presence of motion artifacts, and 15 due to not including the whole breast in the field of view. Therefore, 88 subjects were included in this study, with an average ( $\pm 1$  std. dev.) patient age of  $57 \pm 7$  yr (range 49–75 yr). The average mass glandular fraction of the 88 included subjects was 20% (std. dev. 14%, median 15%).

The corresponding DBT acquisitions resulted in an average CC compressed breast thickness of  $61 \pm 11$  mm (range 30–82 mm) and an average MLO compressed breast thickness of  $59 \pm 12$  mm (range 28–82 mm).

The classification of the cases into the BI-RADS<sup>®</sup> breast density categories was: 3 (BI-RADS<sup>®</sup> A), 34 (BI-RADS<sup>®</sup> B),

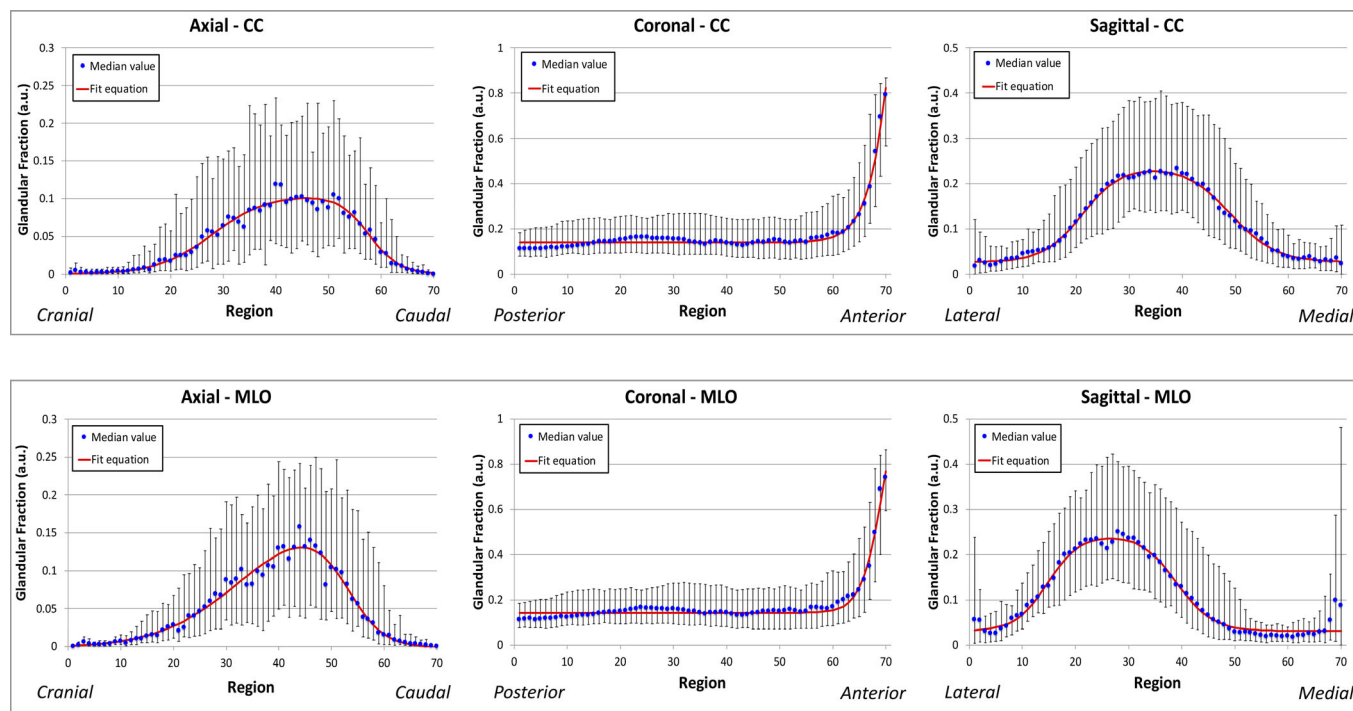


FIG. 4. Glandular fraction distribution in the axial, coronal, and sagittal directions during CC (top panel) and MLO (bottom panel) breast compression. The blue dots represent the median value, the bars represent the 25th and 75th percentiles, and the red line the fit equation. [Color figure can be viewed at [wileyonlinelibrary.com](http://wileyonlinelibrary.com)]

TABLE I. Best fit equation, with parameter values (a, b, c, d, e, and f) for the three fibroglandular tissue distributions for the CC and MLO view. The coefficient of determination ( $r^2$ ) is also reported for both fittings.

$$y = a + \left\{ \frac{b}{1 + \exp[-(x-c+\frac{d}{e})/e]} \right\} \left\{ 1 - \frac{1}{1 + \exp[-(x-c-\frac{d}{e})/e]} \right\}$$

		Axial	Coronal	Sagittal
Craniocaudal	a	0.000168254	0.140544465	0.026394080
	b	0.105393937	6.022672322	0.214081038
	c	42.79228236	73.91495491	35.16729838
	d	29.74072531	1.015183444	27.77828915
	e	5.208161820	2.768884446	3.741112122
	f	2.919379228	6.45031e + 19	4.300551478
	$r^2$	0.975	0.982	0.994
Mediolateral oblique	a	-0.00217112	0.143034161	0.031013211
	b	0.175411300	2.196335279	0.213711071
	c	42.64712232	72.39966645	26.94513554
	d	20.14594310	4.181264152	24.34179369
	e	7.742088982	2.033736314	3.031086481
	f	3.424194197	9.462770989	3.337899539
	$r^2$	0.971	0.972	0.970

33 (BI-RADS® C), and 10 (BI-RADS® D). For eight cases, the BI-RADS® breast density classification was not available. The classification of the cases into the BI-RADS®

assessment distribution at mammographic screening was: 35 (BI-RADS® 0), 49 (BI-RADS® 4), and 4 (BI-RADS® 5).

The results of the analysis of the fibroglandular tissue distribution for the CC and MLO view compression are presented in Fig. 4. Fit equations were the same for all distributions, but with different parameter values, reflecting the tissue distributions for different views and compressions.

As can be seen from the graphs, in the CC view the fibroglandular tissue tends to be more concentrated toward the caudal direction of the breast (about 15% below the breast midplane), and the anterior direction (close to the nipple), and shows a symmetrical distribution in the lateromedial direction.

In the MLO compression, the peak of the fibroglandular tissue distribution in the axial direction is located 3% higher than that in the CC compression, toward the caudal direction of the breast, although it is still about 15% below the breast midplane. More fibroglandular tissue is located in the anterior direction, and with a shift in the lateral direction (about 12% from the center of the breast), making the distribution in this direction non-symmetrical. Fit equations, for both the CC and the MLO case, are reported in Table I.

Figures 5–10 show the results for the additional analyses performed to assess the appropriateness of our methods, especially to exclude biases due to specific characteristics of the dataset, or related to specific processing steps. Figure 5 shows the analysis performed after stratifying the cases

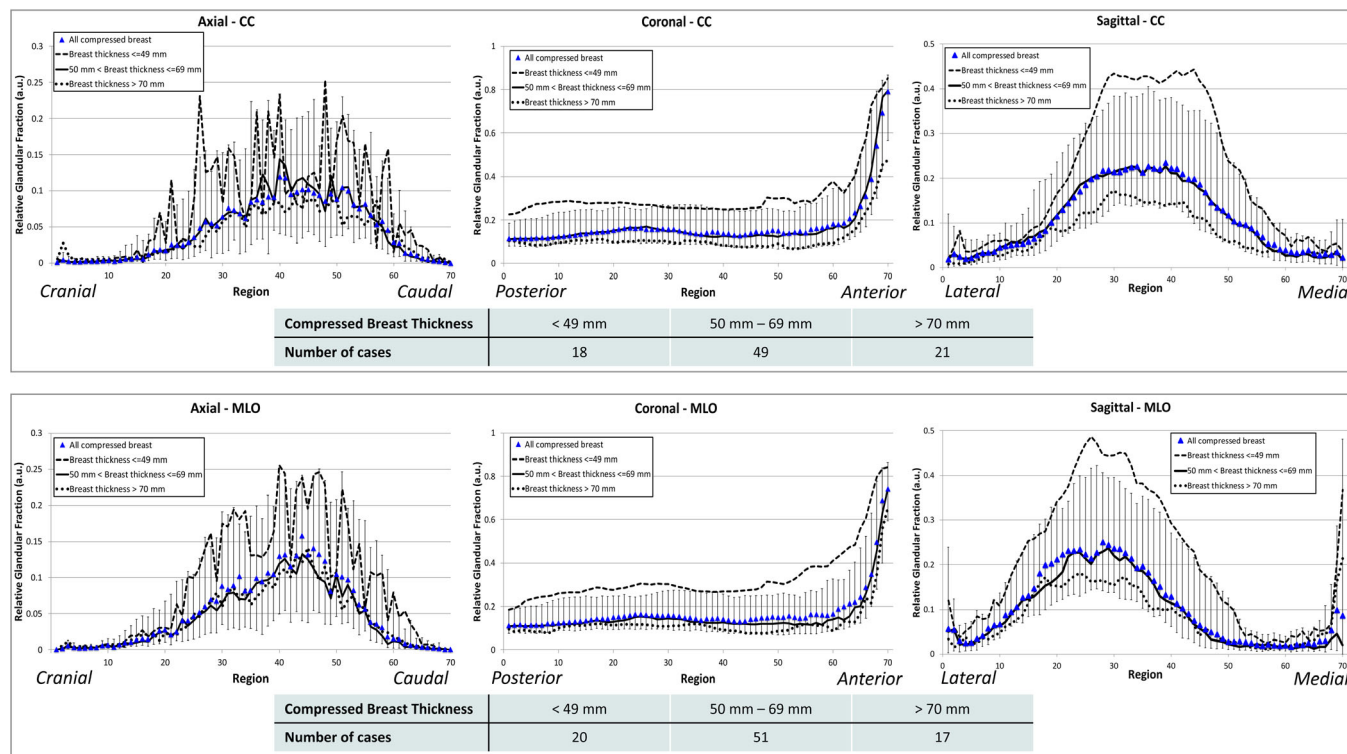


FIG. 5. Glandular fraction distributions for axial, coronal, and sagittal view for the CC (top panel) and MLO breast compression (bottom panel) with patients divided into three compressed breast thickness categories. In each graph the blue triangles represent the median value, while the error bars represent the 25th and 75th percentiles. The dashed line refers to compressed breast thickness lower than 49 mm, the continuous line for compressed breast thickness in the range 50–69 mm, and the dotted line for compressed breast thickness higher than 70 mm. As can be seen, breasts of different thickness follow the same distributions, allowing for the pooling of all the data for the analysis performed. [Color figure can be viewed at wileyonlinelibrary.com]

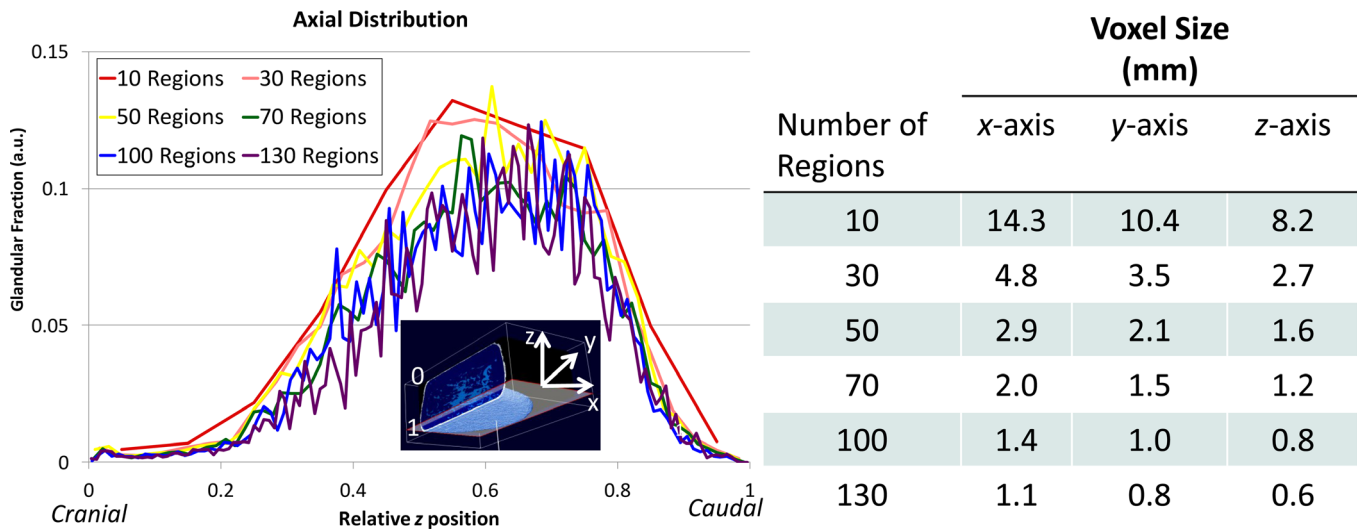


FIG. 6. The graph on the left side shows the behaviour of the axial distribution when the number of regions is increased, and therefore each region is smaller. A higher number of regions leads to a noisier dataset. The inset depicts the axis orientation. The table on the right side lists the voxel size for the largest breast available among the patient-population (i.e.,  $143 \times 104 \times 82 \text{ mm}^3$ ) by number of regions. [Color figure can be viewed at wileyonlinelibrary.com]

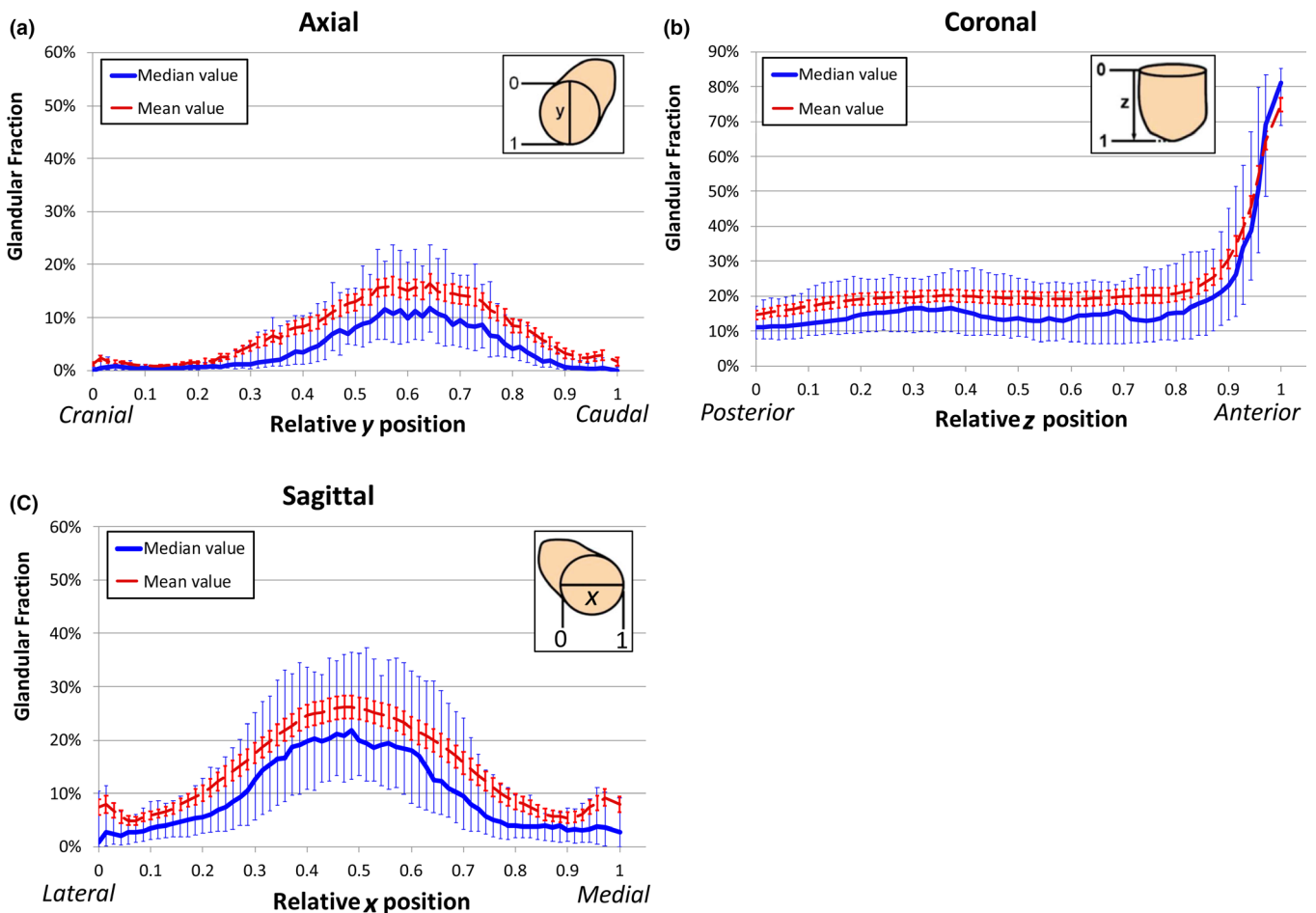


FIG. 7. Glandular fraction distributions for (a) axial, (b) coronal, and (c) sagittal view in the breast before compression. In each graph the blue dots represent the median value, the error bars represent the 25th and 75th percentiles and the red line the fit equation of the mean value. The inset depicts the breast orientation. As can be seen, the bias in the fibroglandular tissue distribution in the axial direction toward the peak density being located below the midplane of the breast is inherent to the breast itself, and not an artifact of the mechanical compression simulation. [Color figure can be viewed at wileyonlinelibrary.com]

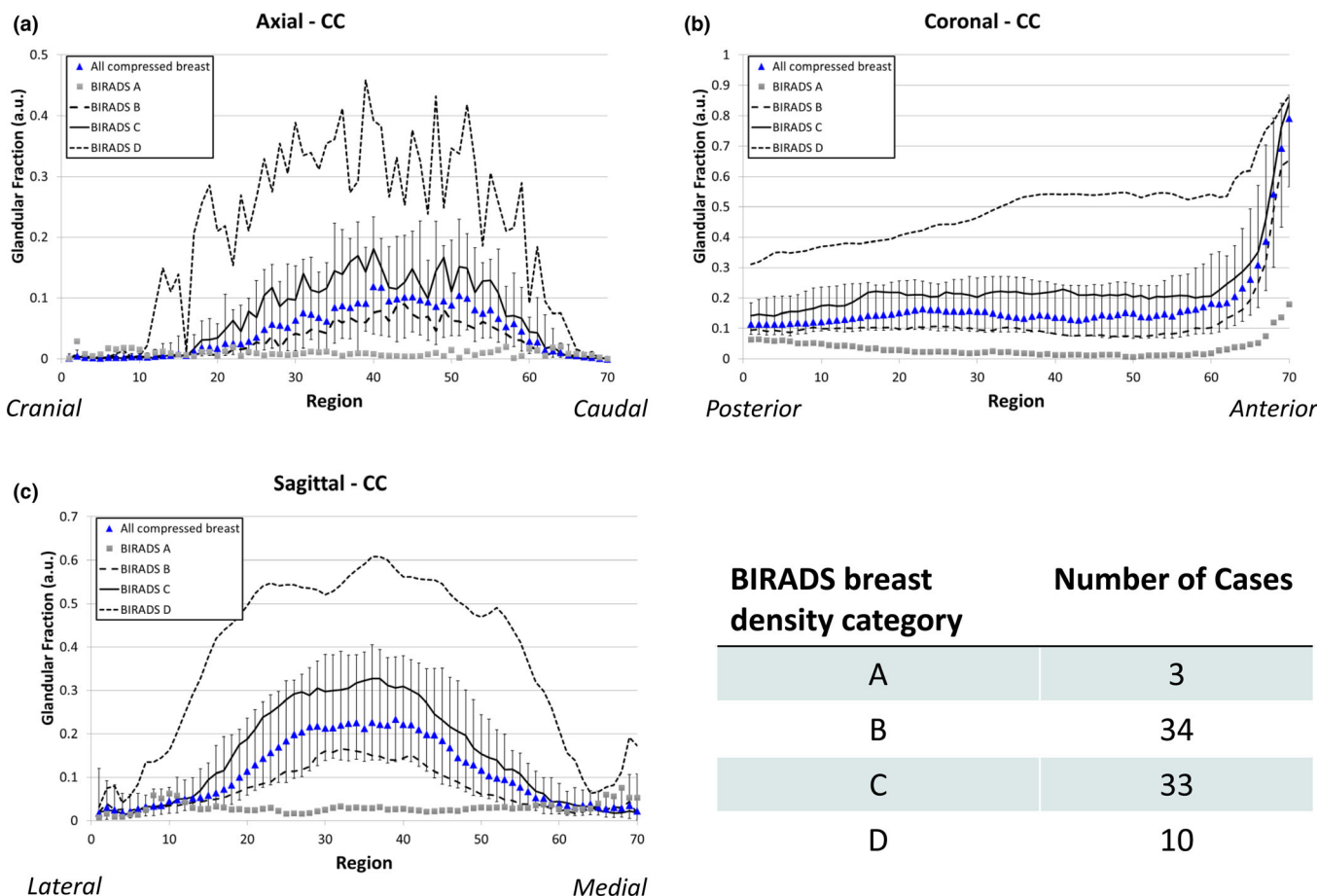


FIG. 8. Glandular fraction distributions for (a) axial, (b) coronal, and (c) sagittal view for the CC breast compression with patients divided according to the BI-RADS<sup>®</sup> breast density categories. The blue triangles represent the median value, while the error bars represent the 25th and 75th percentiles. The analysis was performed using 80 of the 88 cases (for 8 cases, the BI-RADS<sup>®</sup> breast density classification was not available). As can be seen, all groups (except for BI-RADS<sup>®</sup> A) follow the same distributions, allowing for the pooling of all the data for the analysis performed. [Color figure can be viewed at [wileyonlinelibrary.com](http://wileyonlinelibrary.com)]

according to the compressed breast thickness (<49 mm, 50 mm–69 mm, and >70 mm), for both the CC and the MLO view. Figure 6 shows the sensitivity analysis on the number of regions (axial view, uncompressed breasts). Figure 7 shows the analysis performed on the uncompressed-classified breasts. Our results from this latter analysis were concordant with the previous findings of Huang *et al.*<sup>15</sup> performed with a larger dataset, where similar fibroglandular distributions were found. In the coronal direction, the fibroglandular tissue was found to be relatively homogeneously distributed across the whole breast, with a median value below 20%, and with a drastic increase toward the nipple. More importantly, the asymmetry of the fibroglandular tissue distribution in the craniocaudal direction [Fig. 7(a)] can be seen in fig. 13 of Huang *et al.*, with an offset of the peak density by approximately 10% off-center in the vertical section of the sagittal slice.

Figures 8 and 9 show the analysis performed after stratifying the cases according to the presence or absence of mass-like lesions, and according to the BI-RADS<sup>®</sup> breast density category.

Finally, results of the fibroglandular tissue distribution obtained with the Volpara<sup>®</sup> density maps, and their

comparison to the breast CT-obtained distribution, are shown in Fig. 10 and Table II. This analysis was performed for 72 of the 88 cases (for 16 cases the Volpara<sup>®</sup> density maps were not available).

#### 4. DISCUSSION

We characterized the breast parenchyma using patient-based 3D images that were classified and compressed using dedicated simulation algorithms. The images were acquired with dedicated breast CT, a modality specifically designed for breast imaging, and optimized for resolution and contrast requirements of breast tissues. While also other 3D modalities (whole-body CT, MRI) may be used for the same purpose, the characteristics of breast CT allow, to date, for the highest glandular detail depiction, possibly leading to an improved breast tissue characterization.

As opposed to similar previously published studies,<sup>5,6</sup> which either did not account for the compression of the breast,<sup>6</sup> or characterized the dose distribution (and not the tissue distribution) in a limited patient dataset,<sup>5</sup> we investigated the breast glandular distribution in a patient population. This provides information that may aid researchers in developing



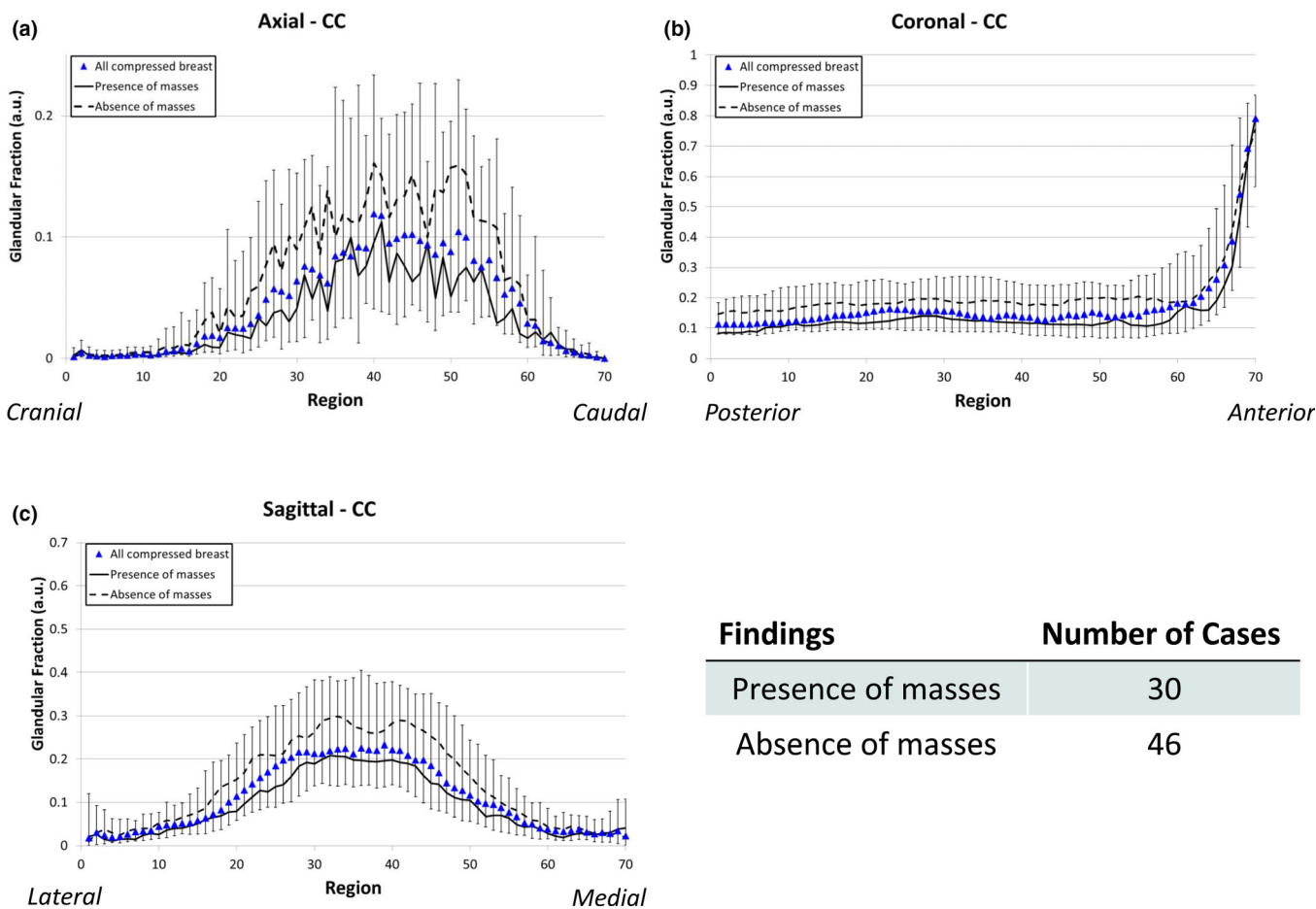


FIG. 9. Glandular fraction distributions for (a) axial, (b) coronal, and (c) sagittal view for the CC breast compression with patients divided according to the presence of mass findings. The blue triangles represent the median value, while the error bars represent the 25th and 75th percentiles. The dashed line refers to compressed breast containing mass findings (overall glandular fraction — mean  $\pm$  1 standard deviation: 15.2%  $\pm$  7.4%), and the dotted line to compressed breast without mass findings (overall glandular fraction — mean  $\pm$  1 standard deviation: 25.7%  $\pm$  17.2%). The analysis was performed using 76 of the 88 cases (for 12 cases, the type of finding was not available). As can be seen, both groups follow the same distributions, allowing for the pooling of all the data for the analysis performed. [Color figure can be viewed at [wileyonlinelibrary.com](http://wileyonlinelibrary.com)]

an accurate breast dose evaluation and more advance breast cancer risk models.<sup>24</sup>

Our findings indicate that the fibroglandular tissue tends to concentrate below the midplane of the breast, that is, in the caudal direction, with the glandularity being higher in regions located close to the nipple. Meanwhile, regions close to the skin and the chest wall showed a sparse fibroglandular tissue concentration. Interestingly, while dense regions appeared to be distributed symmetrically in the sagittal direction in the CC-view compressions, in the case of the MLO higher density was found in the lateral side of the breast compared to the medial. However, this can be explained by assessing how the dense tissue distribution, as existent in the uncompressed (see Fig. 7) or CC-view compressed breast, would behave when compressed at an angle for the MLO-view positioning.

Our results confirm the need to review the breast model used to estimate the radiation dose during mammography and DBT, since a higher amount of fibroglandular tissue located in the most caudal area of the breast leads to a lower radiation dose, due to the shielding effect of the tissue present toward the incident x-ray side.<sup>7</sup>

The comparison between the compressed breast CT data and the Volpara<sup>®</sup> density maps (Fig. 10) resulted in similar tissue distributions in the coronal direction. In the sagittal direction, the distributions obtained from the Volpara<sup>®</sup> density maps showed less variation throughout the breast than that in the compressed breast CT volumes. This resulted in higher local glandular fractions in the lateral and medial regions (MLO view), and lower in the central area of the breast (both CC and MLO views). Nevertheless, while different in amplitude, the main characteristics of the distribution are similar to those obtained with the breast CT data. Specifically, the overall symmetry/asymmetry of the distributions (depending on the view and direction), the location of the peak in the asymmetric density distributions, and the overall width of these peaks were consistent. Therefore, while the Volpara<sup>®</sup> density maps cannot be considered as an absolute ground truth either (due to the uncertainty in their accuracy, and more importantly, to the lack of any information in the third dimension), this does suggest that the compression algorithm used in this study may result in a correct model for the displacement of the tissue in a population of breast volumes.

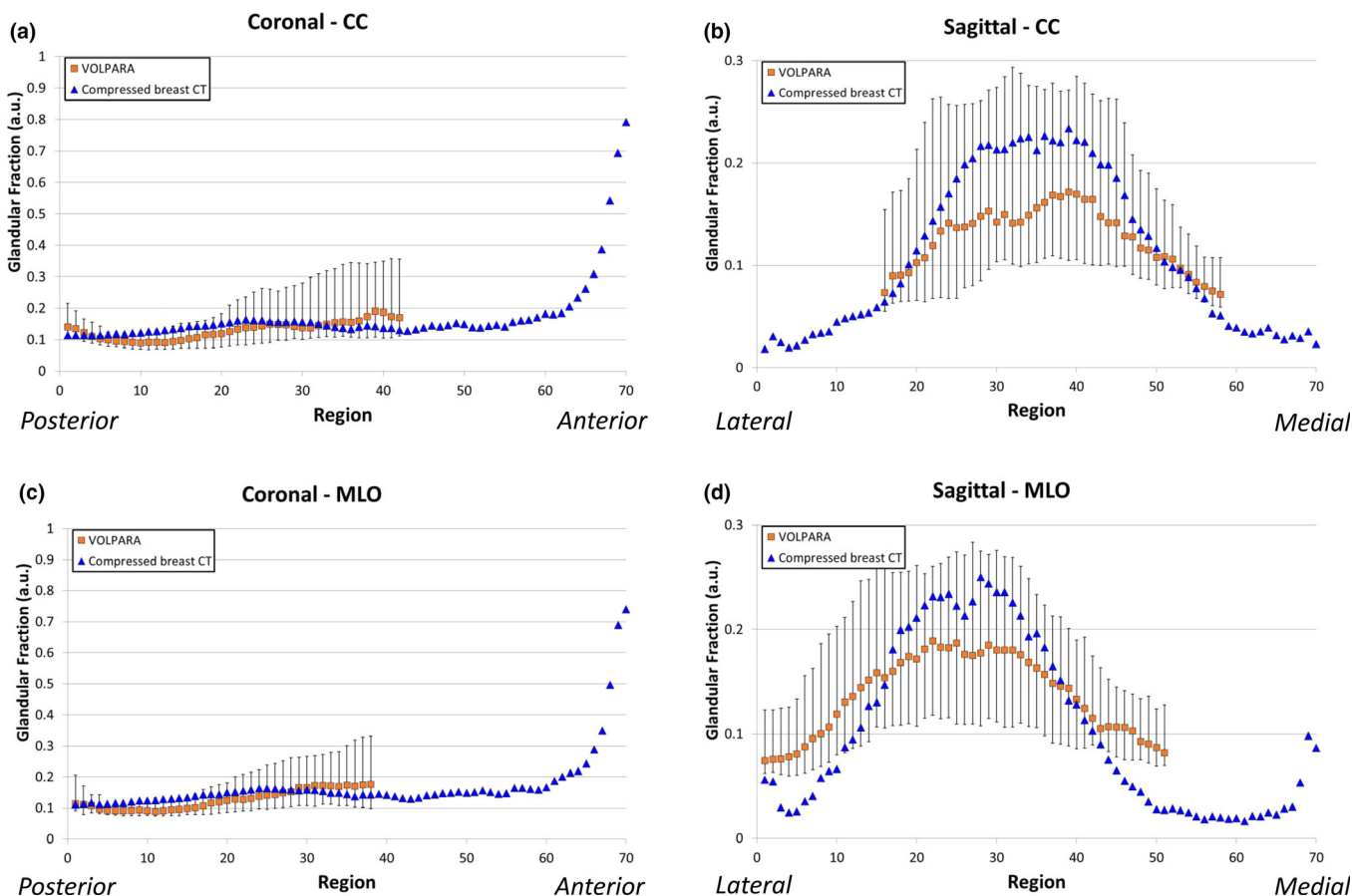


FIG. 10. Glandular fraction distributions for (a), (c) coronal and (b), (d) sagittal views for the CC and MLO breast compressions, obtained from the compressed breast CT data and from the Volpara® density maps of the corresponding mammograms. The orange squares represent the median value of the distribution obtained with the Volpara® density maps, while the error bars represent the 25th and 75th percentiles. The blue triangles represent the median value of the distribution obtained from the compressed breast CT data. The Volpara® analysis was limited to the inner breast region, where the 2D density maps assume a constant compressed breast thickness, avoiding the breast periphery where the compressed thickness varies due to the breast curvature. [Color figure can be viewed at wileyonlinelibrary.com]

TABLE II. Peak position and full-width-at-half-maximum of the sagittal distributions (Gaussian fit) extracted from the compressed breast CT images and from the Volpara® density maps.

	CC view		MLO view	
	Breast CT	Volpara®	Breast CT	Volpara®
Peak position (region num.)	37	36	26	25
Full-width-at-half-maximum (# regions)	34	38	30	39

The main limitation of this study is the relatively small size of the image dataset, due to breast CT still being an imaging modality used only at very few centers around the world, and not yet fully implemented in the daily clinical routine. However, as can be seen in Figs. 5, 8, and 9, analyses of the distribution with a portion of the dataset with different breast thicknesses, different overall densities, and the presence or absence of mass finding already show the same distribution characteristics. This seems to suggest that the inclusion of additional cases would not significantly modify

our results. Moreover, our results are concordant with previous findings obtained for a larger uncompressed breast dataset representing a different patient population,<sup>15</sup> and therefore represent a substantial improvement over the models currently used worldwide for routine breast dosimetry.

Another two limitations are related to the hardware and software algorithms used to perform our analysis, including the finite spatial resolution of the dedicated breast CT system (and consequent partial volume effect), and potential small uncertainties deriving from the tissue classification algorithms. These include, for example, voxel misclassification in regions located close to the skin layer, and at the boundary between fibroglandular and adipose tissue. While future studies with larger image datasets could help compensate for any inaccuracies introduced, the choice of dividing the compressed breast into 70 macroregions in each orthogonal direction, as opposed to evaluating the distribution per voxel, limits any potential errors arising when calculating the breast glandularity.

Finally, the simulation of the mechanical compression of the breast presents the limitation that it does not take into account the manual handling of the breast by the technologist

during positioning (e.g., stretching of the breast), in addition to including some assumptions on tissue elasticity and the compression process itself.<sup>18</sup> This might, in principle, influence the distribution of the fibroglandular tissue. However, an analysis of the fibroglandular tissue distribution on the same patient breast dataset but without the simulated mechanical compression shows similar results, that is, more dense tissue concentrated toward the caudal and anterior directions (see Fig. 7). Therefore, this indicates that the compression simulation probably does not introduce a bias in the distribution of the fibroglandular tissue.

In a recent preliminary study,<sup>25</sup> the distributions presented in this work were used to estimate the radiation dose in digital mammography, and results pointed to a dose reduction of approximately 30% compared to the currently used homogeneous model. Although preliminary, these findings suggest that incorporating the spatial variation of the fibroglandular tissue can lead to improvements in delivered radiation dose estimates, potentially helping develop accurate dose models that better account for the breast anatomy as seen in breast CT.

In future work, the potential benefit, from a dosimetric perspective, of the proposed patient-based breast density model will be investigated further. This includes the generation of digital phantoms that replicate the spatially varying fibroglandular tissue distribution, and their comparison against homogenous phantoms, for multiple breast shapes, thicknesses, and overall density values.

## 5. CONCLUSIONS

We have characterized the fibroglandular distribution of the breast during mammographic and DBT imaging, using dedicated breast CT patient images with isotropic spatial resolution, and a series of image processing algorithms, including mechanical breast compression simulation. The resulting breast models include a nonuniform and asymmetric fibroglandular distribution, reflecting the characteristics identified in the patient data. This understanding could be used to improve radiation dosimetry models and their corresponding risk, by the future development of phantoms that replicate the patient-based fibroglandular distribution for multiple overall glandular fractions, and their comparison (in terms of dose) with the currently used homogeneous model. In addition, this study might provide further insight on how the location of dense breast tissue, and not only its amount, relates to breast cancer development risk.

## ACKNOWLEDGMENTS

This research was supported in part by grant R01CA181171 from the National Cancer Institute, National Institutes of Health, and grant IIR13262248 from the Susan G. Komen Foundation for the Cure. The content is solely the responsibility of the authors and does not necessarily represent the official views of the National Cancer Institute, the National Institutes of Health, or the Komen Foundation. The

authors would like to acknowledge Gerrita van Spijker for her support provided in data collection, and Melissa Hill for her input and feedback on the use of the Volpara<sup>®</sup> software.

## CONFLICT OF INTEREST

The authors have no relevant conflict of interest to disclose.

## DATA AVAILABILITY STATEMENT

The data generated and/or analysed during the current study are available from the corresponding author on reasonable request.

\*Christian Fedon and Marco Caballo equally contributed to this work, as co-first authors.

<sup>a)</sup>Author to whom correspondence should be addressed. Electronic mail: Ioannis.Sechopoulos@radboudumc.nl.

## REFERENCES

- McCormack VA, Dos Santos SI. Breast density and parenchymal patterns as markers of breast cancer risk: a meta-analysis. *Cancer Epidemiol Biomark Prev.* 2006;15:1159–1169.
- Ng KH, Lau S. Vision 20/20: mammographic breast density and its clinical applications. *Med Phys.* 2015;42:7059–7077.
- Boyd NF, Guo H, Martin LJ, et al. Mammographic density and the risk and detection of breast cancer. *N Engl J Med.* 2007;356:227–236.
- Dance DR, Hunt A, Bakic PR, et al. Breast dosimetry using high-resolution voxel phantoms. *Radiat Prot Dosim.* 2005;114:359–363.
- Sechopoulos I, Bliznakova K, Qin X, Fei B, Feng SSJ. Characterization of the homogenous tissue mixture approximation in breast imaging dosimetry. *Med Phys.* 2012;39:5050–5059.
- Hernandez AM, Seibert JA, Boone JM. Breast dose in mammography is about 30% lower when realistic heterogeneous glandular distribution are considered. *Med Phys.* 2015;42:6337–6348.
- Dance DR, Sechopoulos I. Dosimetry in x-ray-based breast imaging. *Phys Med Biol.* 2016;61:R271–R304.
- Himes DO, Root AE, Gammon A, Luthy KE. Breast cancer risk assessment: calculating lifetime risk using the Tyrer-Cuzick model. *J Nurse Pract.* 2016;12:581–592.
- Santiago-Rivas M, Benjamin S, Jandorf L. Breast density knowledge and awareness. *J Prim Care Community Health.* 2016;7:207–214.
- Yaffe MJ. Mammographic density. Measurement of mammographic density. *Breast Cancer Res.* 2008;10:209–218. <https://doi.org/10.1186/bcr2102>
- Wengert GJ, Helbich TH, Leithner D, Morris EA, Baltzer PAT, Pinker K. Multimodality imaging of breast parenchymal density and correlation with risk assessment. *Curr Breast Cancer Rep.* 2019;11:23–33.
- Gastouniotti A, McCarthy AM, Pantalone L, Synnestvedt M, Kontos D, Conant EF. Effect of mammographic screening modality on breast density assessment: digital mammography versus digital breast tomosynthesis. *Radiology.* 2019;291:320–327.
- Sechopoulos I. A review of breast tomosynthesis. Part I. The image acquisition process. *Med Phys.* 2013;40:014301.
- Sechopoulos I, Feng SSJ, D'Orsi CJ. Dosimetry characterization of a dedicated breast computed tomography clinical prototype. *Med Phys.* 2010;37:4110–4120.
- Huang SY, Boone JM, Yang K, et al. The characterization of breast anatomical metrics using breast CT. *Med Phys.* 2011;38:2180–2190.
- Yaffe MJ, Boone JM, Packard N, et al. The myth of the 50–50 breast. *Med Phys.* 2009;36:5437–5443.
- Caballo M, Boone JM, Mann R, Sechopoulos I. An unsupervised automatic segmentation algorithm for breast tissue classification of dedicated breast computed tomography images. *Med Phys.* 2018;45:2542–2559.

18. Fedon C, Rabin C, Caballo M, et al. Monte Carlo study on optimal breast voxel resolution for dosimetry estimates in digital breast tomosynthesis. *Phys Med Biol.* 2019;64:015003.
19. García E, Fedon C, Caballo M, Martí R, Sechopoulos I, Diaz O. Realistic compressed breast phantoms for medical physics applications. *Proc IWBI*; 2020:1151304.
20. García E, Diaz O, Martí R, et al. Local breast density assessment using reacquired mammographic images. *Eur J Radiol.* 2017;93:121–127.
21. Highnam R, Brady SM, Yaffe MJ, et al. Robust Breast Composition Measurement - VolparaTM. *IWDM 2010*. Lecture Notes in Computer Science, vol 6136. Springer, Berlin, Heidelberg.
22. Huang SY, Boone JM, Yang K, Kwan AL, Packard NJ. The effect of skin thickness determined using breast CT on mammographic dosimetry. *Med Phys.* 2008;35:1199–1206.
23. Branderhorst W, de Groot JE, van Lier MGJTB, Highnam RP, den Heeten GJ, Grimbergen CA. Technical note: validation of two methods to determine contact area between breast and compression paddle in mammography. *Med Phys.* 2017;44:4040–4044.
24. Yaffe MJ, Mainprize JG. Risk of radiation-induced breast cancer from mammographic screening. *Radiology.* 2011;258:98–105.
25. Arana Peña LM, Fedon C, Garcia E, et al. Monte Carlo dose evaluation of different fibroglandular tissue distribution in breast imaging. *Proc IWBI*; 2020:11513.